Comparison of Linear Unmixing Methods on Paintings Data Set

Jizhen Cai, Hermine Chatoux, Clotilde Boust, Alamin Mansouri

Comparison of Linear Unmixing Methods on Paintings Data Set

Jizhen Cai[1] Hermine Chatoux[1] Clotilde Boust[2] Alamin Mansouri[1]

[1] Laboratoire Imagerie et Vision Artificielle, Universite Bourgogne Franche-Comté
[2] Le Centre de Recherche et de Restauration des Musées de France (C2RMF)

9, Avenue Alain Savary, 21000 Dijon, France
Jizhen_Cai@etu.ubourgogne.fr

Résumé

Le démélangeage hyperspectral consiste à extraire des endmembers puis déterminer l'abondance des endmembers dans chaque pixel de l'image. Dans cet article, nous présentons trois méthodes de l'état de l'art pour extraire les endmembers. Ces méthodes sont habituellement utilisées dans le domaine de la télédétection. Elles sont ici appliquées à un nouveau domaine : le patromoine culturel. Les méthodes sont testées sur une base de données peinture. Nous comparons et analysons les résultats et performances de ces méthodes sur ce type de données.

Mots Clef

Hyperspectral Unmixing, Extraction des endmembers

Abstract

Hyperspectral unmixing consists in extracting Endmembers and estimating the abundance of each Endmember in each pixel of the images. In this article, we present three state of the art methods in Endmembers Extraction. These methods are originally used in the field of remote sensing. They are applied to a new domain: paintings. We compare and analyze their performances and results.

Keywords

Hyperspectral Unmixing, Endmember Extraction.

1 Introduction

Hyperspectral Unmixing (HU) has been intensely discussed, especially in the field of Remote Sensing. Wang *et al.* [24] defined Hyperspectral Unmixing as the procedure to obtain the spectra (called *Endmember*) that constituted the hyperspectral images (HSIs) and the corresponding proportion of each endmember (called *Abundance*). The algorithms of spectral unmixing heavily depend on the situation of mixing. According to Bioucas-Dias *et al.* [4], Hyperspectral Unmixing can be classified as Linear Mixture Model or Non-linear Mixture Model.

In real cases, as Bioucas-Dias *et al.* [4] have concluded, the Linear Mixture Model is more widely used. In fact, when the scattering effects and the interactions among different materials (endmembers) are not macroscopic and significant, the Linear Mixture Model is more appropriate. It can be expressed as follow:

$$Y = EA + \epsilon = \begin{pmatrix} e_{1,1} & \dots & e_{1,P} \\ \vdots & \ddots & \vdots \\ e_{L,1} & \dots & e_{L,P} \end{pmatrix} \times \begin{pmatrix} a_1 \\ \vdots \\ a_P \end{pmatrix} + \epsilon \quad (1)$$

where Y= $[y_1, ..., y_L]^T$ is a pixel of a hyperspectral image, E is a L $\times$ P matrix describing the P endmembers in the L bands, A corresponds to the abundances of P endmembers for the pixel Y, and ϵ is a L $\times$ 1 vector which corresponds to the noise.

On the contrary, when the interactions among the different endmembers cannot be ignored, the Non-linear Mixture Model is more likely to obtain better results. The advantage of Non-linear Mixture Model is that it takes the interactions among the endmembers into considerations. The Generalized Bilinear Model (GBM) which was proposed by Halimi *et al.* [14] can be a good example of Non-linear Mixing Model, which can be expressed as follow:

$$Y = EA + \sum_{i=1}^{P-1} \sum_{j=i+1}^{P} (e_i \circ e_j) + \epsilon, \quad (2)$$

where $\circ$ denotes the element-wise multiplication between two vectors.

In past few decades, the Hyperspectral Unmixing has been applied in various domains including rock and soil classification [1], vegetation phenology [11], crop yield [27]. However, its application upon the painting is relatively new. Even though in the past few years, some relevant researches have been published. For example, in 2021, Deborah *et al.* [10] have studied the performance of Abundance Estimation Model *Fully Constrained Least Squares* on the painting of *Scream*. In 2021, Grillini *et al.* [12] have compared the performances of various Abundance Estimation Models upon a mockup painting. These researches mostly focus on the Abundance Estimation Models. In fact, the unmixing methods, which extract the endmembers, are even more fundamental and important, but the research focusing on the Unmixing Methods is quite scarce.

The remainder of the article is structured as follows. Section 2 introduces the widely-used Endmember Extraction methods and Abundance Estimation models in remote sensing. Section 3 introduces the Experimental Protocol of this article and the spectral comparison metrics we are going to utilize. Section 4 shows the implementation of Endmember Extraction methods upon the paintings data set and analyze of the results. Finally, we conclude the paper.

2 Unmixing Methods

The procedure of Hyperspectral Unmixing can be roughly divided into three major steps: Estimation of the number of the endmembers, Endmember Extraction, Estimation of the Abundance of all pixels. We are only interested in the last two step in this article.

Firstly, the data sets of hyperspectral images are high-dimensional data. Therefore, most of the researchers apply some dimension reduction methods as preprocessing step. For example in research of Licciardi and Del Frate [19], the authors adopt PCA to reduce the dimension of data in advance, which reduces the calculation time. Secondly, the Endmember Extraction is applied to obtain the endmembers which are often the pure pixels in the data set. As it is mentioned above, the target of Hyperspectral Unmixing is to find out all the endmembers and their corresponding abundances in the images. Therefore, the step of Endmember Extraction is the most important part of Hyperspectral Unmixing, since it affects greatly the results in Abundance Estimation. Thirdly, different Abundance Estimation models with different constraints are applied to figure out the corresponding abundances of each endmember in each pixel.

2.1 Finding Endmembers

We will now present the three Endmember Extraction methods which are implemented in this article. These three methods are chosen for two reasons. Firstly, they are all the popular endmember extraction methods which are widely recognized and utilized. Secondly, they are based on different assumptions and constraints, implying different performances according to different situations. For instance, although VCA, N-FINDR share the assumption that pure pixels exist in the data set, their algorithms are totally different. VCA deals with the problem from the direction of projection, while N-FINDR studies the problem from the calculation of the multi-dimension Volume. At the same time, NMF does not have the constraint of the existence of pure pixels. Besides, as Lu *et al.* [20] suggested, NMF sufficiently utilized the sparse characteristic of the data, which gave NMF the advantage to extract local semantic information.

2.1.1 Vertex Component Analysis (VCA)

VCA is an unsupervised method that deals with the problem of endmember extraction in Hyperspectral Images. This method was firstly presented by Nascimento and Dias [21]. This method is based on the assumption that pure pixels exist in the data set. Because of that, the endmembers will always be the vertices of a simplex. VCA finds the most suitable endmembers by iteratively projecting data onto the direction orthogonal to the subspace which is already spanned by the endmembers determined.

Chang [5] pointed out that the limit of VCA was due to the fact that it required to generate random vectors for extracting initial endmembers. This randomness in the initialization made it difficult for VCA to repeatedly get the same results each time.

2.1.2 N-FINDR

N-FINDR is a spectral unmixing method which was proposed by Winter [25]. The method originates from the fact that in the P spectral dimensions, there can be myriads of P-Volume. But among all of them, the largest volume can only be obtained when we utilize the purest endmembers for such P-Volume.

The Endmember Matrix can be expressed as:

$$E' = \begin{pmatrix} 1 & 1 & ... & 1 \\ e_{1,1} & e_{1,2} & ... & e_{1,P+1} \\ ... & ... & ... & ... \\ e_{P,1} & e_{P,2} & ... & e_{P,P+1} \end{pmatrix}, \tag{3}$$

where E′ is a (P+1) × (P+1) matrix, P stands for the number of Endmembers. In that case, as defined by Stein [23], the P-Volume of this Endmember Matrix E′ can be expressed as:

$$|\mathcal{V}(\overrightarrow{E'})| = \frac{1}{P!}|\det(E')|, \tag{4}$$

where $|\mathcal{V}(\overrightarrow{E'})|$ denotes the P-volume of these endmembers and det(.) denotes the determinant.

As Chang *et al.* [6] have figured out, there exists a limit for N-FINDR: it needs to generate initial random values, which makes it hard to guarantee the repeatability. Besides, N-FINDR requires more calculation than VCA.

2.1.3 NMF

Non-negative Matrix Factorization (NMF) was originally presented by Lee and Seung [18] as a brand new method in tackling the problem of learning parts of semantic features from image. Traditionally, the feature extraction methods like Principal Component Analysis (PCA) extract endmembers without considering the information from a local view. On the contrary, NMF has overcome such disadvantage by only permitting non-negative values in the matrices, which makes it an additive combination of all parts of the images. When NMF is applied upon the field of spectral analysis, it can be expressed as follow:

$$Y = EA, \tag{5}$$

where Y, E, A are all Non-negative Matrices. Y is a L × N matrix containing the reflectance of all N pixels in the L bands. E is a L × P matrix describing the P endmembers

in the L bands. A is a P $\times$ N matrix describing the corresponding abundances of P endmembers in the N pixels. When a non-negative matrix Y is gotten, the goal is to find out the most suitable values in non-negative matrix E and A. This goal is achieved, when the Cost Function below can get its Minimum Value.

$$\min_{E,A} ||(Y - EA)||^2. \tag{6}$$

As Albright *et al.* [2] pointed out, NMF had the problem of finding global minimum. In other words, when NMF is applied, what we get is a local minimum. This is due to the fact that cost function cannot guarantee the convex of E, A in equation 5 at the same time.

2.2 Finding Abundances

In this section, we discuss the models of extracting the abundance. As Dalla *et al.* [8] put forward in their paper, several methods were often utilized: Unconstrained Least Squares (UCLS), Non-negative Constrained Least Squares (NCLS) and Fully Constrained Least Squares Unmixing (FCLSU). The Table 1 presents which methods respond to which constraints.

These methods of finding abundances distinguish themselves from each other by the constraints they are imposing on the abundance coefficients. The Abundance Non-negativity (ANC) implies the abundances to be positive or null:

$$\alpha_i \geq 0, i \in \{1, 2, 3, ..., P\}. \tag{7}$$

The condition of ANC suggests that the endmembers can be present or not, but all of them cannot have negative contribution to the final result.

Meanwhile, the condition of Abundance Sum-to-one Constraints (ASC) requires that the Endmembers' Abundances sum to one:

$$\sum_{i=1}^{P} \alpha_i = 1. \tag{8}$$

Table 1: Finding Abundance methods with constraints

Methods	**ANC**	**ASC**
UCLS	Not Satisfied	Not Satisfied
NCLS	Satisfied	Not Satisfied
FCLSU	Satisfied	Satisfied

3 Similarity Measures

The experimental procedure consists in three steps. In the first step, we apply the Endmember Extraction Methods including VCA, NMF, N-FINDR upon the painting data described in Section 4, to extract the endmembers. Secondly, the extracted endmembers are compared with the ground-truth endmembers using the spectral comparison metrics mentioned below. Thirdly, the corresponding abundances calculated using the extracted endmembers are compared with the ground-truth abundances using the metric of SAVD. SAVD is not a spectral comparison metric. Instead, it is an index based on L1-norm. That is why we do not include it in this section.

In this section, We will present three different metrics for spectral comparison. These three metrics, SAM, SID and MAPE are chosen for two reasons. Firstly, they prove to be useful for various situations. Secondly, each of them has its own advantages and disadvantages.

As Kruse *et al.* [16] suggested, SAM only utilized the vector "direction" of the spectra and not their vector "length", therefore the method is insensitive to illumination and albedo effects. Meanwhile, SID has overcome the disadvantage of SAM. Thus, SID is more robust and effective in subtle spectral difference. However, the results of SAM are confined between 0 and π, while the results of SID do not have such limits. This feature has made the results of SAM more explicit than those of SID. At the same time, unlike SAM and SID, the Mean Absolute Percentage Error (MAPE) measures the accuracy of Extracted Endmember from another perspective. The use of MAPE is necessary, because SAM and SID only measure the difference between different spectra. However, sometimes, we also need have an intuitive understanding of the degree of similarity between spectra. As Kim and Kim [15] noted, MAPE had the advantages of scale-independency and interpretability. Based on such consideration, we maintain that the MAPE is essential as one metric.

3.1 Spectral Angle Mapper (SAM)

SAM is one of the most commonly used indicator for spectral difference comparison. This method was firstly introduced by Yuhas *et al.* [28]. The core idea of SAM is to compare two spectra by measuring the angle between these two vectors. A smaller angle suggests more similarity between these two spectra.

$$\alpha = \arccos\left(\frac{\sum_{k=1}^{L} r_k t_k}{\sqrt{\sum_{k=1}^{L} r_k^2}\sqrt{\sum_{k=1}^{L} t_k^2}}\right), \tag{9}$$

where t_k is the test spectrum in k^{th} band; r_k is the reference spectrum in k^{th} band; L denotes the total number of bands in the data set.

3.2 Spectral information divergence (SID)

SID was inspired from the Kullback–Leibler measure of information, which was firstly proposed by Kullback and Leibler [17]. However, as Perez-Cruz [22] has noticed, there exists a lack of symmetry in this measure. They pro-

pose a symmetric writing:

$$SID(R,S) = \sum_{k=1}^{L} r_k log(\frac{r_k}{t_k}) + \sum_{k=1}^{L} t_k log(\frac{t_k}{r_k}). \quad (10)$$

3.3 Mean Absolute Percentage Error (MAPE)

MAPE is a popular statistical index. As De *et al.* [9] pointed out, MAPE had the advantage of very intuitive interpretation in terms of relative error, when the quantity to predict was known to be above zero. Our data set satisfies the requirement well. This is why MAPE is a very appropriate metric for our data. Briefly, MAPE can be defined as follow:

$$MAPE = \frac{1}{L} \sum_{k=1}^{L} \frac{|t_k - r_k|}{r_k} \times 100\%. \quad (11)$$

4 Experiment on Paintings Data set

Here we use an open data set that was presented by Grillini *et al.* [13]. In this data set, there are seven different pigments including *Vermilion*, *Gold Ochre DD*, *Ultramarine Blue*, *Kremer White*, *Carmine*, *Naples Yellow*, *Viridian Green*. As the Figure 1 shows, there are 175 painted patches. Each 2cm $\times$ 2cm patch is either a pure pigment or the mixture of 2 or 3 pigments. Indeed, it is rare to find a mix of more than 3 pigments in the mixture of traditional oil painting. Yet, no constraint on the number of pigment is set on the Abundance extraction which can be from one to seven.

In this data set, the ground-truth spectra of these seven pure pigments (as Figure 2 shows), the spectra of all the 175 color patches and corresponding abundances are given.

In Figure 3, we choose to demonstrate the unmixing results of *Ultramarine Blue* and *Carmine*. In fact, from Figure 3, it's very intuitive that *Ultramarine Blue* is well extracted, *Carmine* is comparatively badly extracted using these three unmixing methods.

For the extraction of the *Ultramarine Blue* endmembers, all methods give a spectra that are similar to the ground truth. The VCA method extract a spectra that is, qualitatively, closer to the ground truth than other methods. It is confirmed by the similarity measure which is the smallest for the *Ultramarine Blue* pigment extracted by the VCA as shown in Table 3 to 4.

On the contrary, the *Carmine* endmembers extracted are far from the ground truth. The N-FINDR method has a closer shape than the other methods. Yet, only the MAPE similarity measure gives a better results to the N-FINDR method.

From Table 3 to 4, we can notice that extreme values exist in certain pigments, especially when we apply VCA and N-FINDR. For example, the 241.5% of *Kremer White* and the 142.0% of *Viridian Green* when using VCA. As Cui *et al.* [7] have mentioned in their research, most endmember extraction methods do not consider the spatial adjacency, but

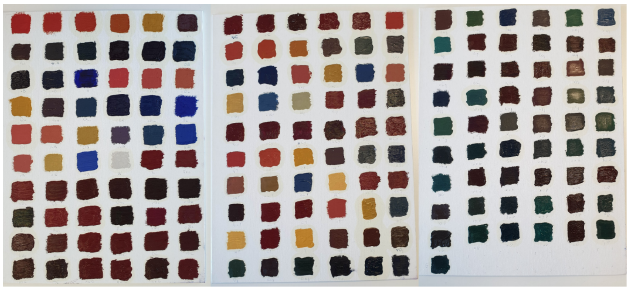

Figure 1: Illustration of the 175 painted patches

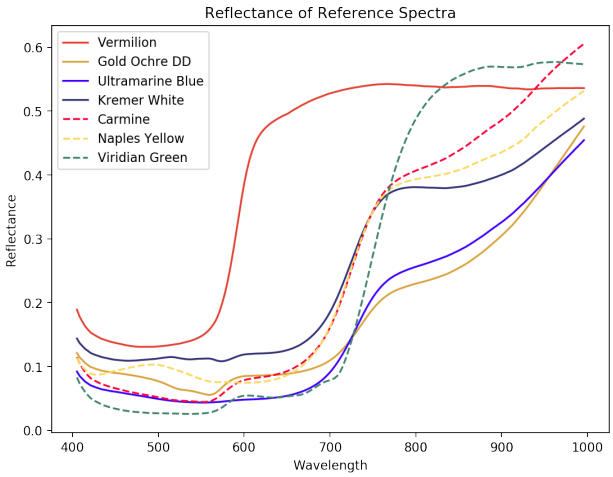

Figure 2: Reflectance of reference spectra of the seven pigments in the color patches.

problem of the mixing oil has some connections with spatial adjacency and Non-linear Mixing. Thus, endmember extraction methods may fail to obtain excellent and robust results on such data set. That is why, in the following of the article, we will focus moslty on the MAPE similarity measure.

Additionally, we also need one metric for evaluating these models' performances in Abundance Estimation. In that case, here we define SAVD (Sum of the Absolute Value of Difference between Estimation Abundance and Ground Truth Abundance) as the metric for evaluating the model's performance in Abundance Estimation. SAVD is constructed from the idea of L1-norm. Here we have adopted L1-norm instead of L2-norm, because as Bektas and Sisman [3] have figured out, L1-norm is more robust than L2-norm. SAVD can be defined as below:

$$SAVD = \sum_{k=1}^{P} |EA_k - GTA_k|, \quad (12)$$

where P means the the number of pigments (endmembers) in this mixture. EA_k means the estimation abundance of k^{th} pigment. GTA_k means the ground truth abundance of k^{th} pigment. Table 5 presents the minimum, maximum, average and standard deviation of the SAVD associated to the abundance extracted. From this table, no methods

Table 2: The SAM between Ground Truth Endmembers and Extracted Endmembers on Paintings Data set

Spectral Angle Mapper (SAM)			
Endmember	VCA	NMF	N-FINDR
Vermilion	0.580	0.364	0.105
Gold Ochre DD	0.523	0.408	0.363
Ultramarine Blue	0.088	0.268	0.163
Kremer White	0.342	0.319	0.066
Carmine	0.622	0.203	0.467
Naples Yellow	0.400	0.911	0.393
Viridian Green	0.424	0.958	0.086
Average of 7 endmembers	0.413	0.490	0.235

Table 3: The SID between Ground Truth Endmembers and Extracted Endmembers on Paintings Data set

Spectral Information Divergence (SID)			
Endmember	VCA	NMF	N-FINDR
Vermilion	58.6	102	3.00
Gold Ochre DD	31.0	25.8	28.1
Ultramarine Blue	1.80	9.87	7.45
Kremer White	18.5	32.0	1.65
Carmine	5.30	23.3	29.3
Naples Yellow	104	84.6	29.3
Viridian Green	18.0	101	2.72
Average of 7 endmembers	33.9	54.1	14.5

Table 4: The MAPE between Ground Truth Endmembers and Extracted Endmembers on Paintings Data set

Mean Absolute Percentage Error (MAPE)			
Endmember	VCA	NMF	N-FINDR
Vermilion	37.07%	81.34%	19.63%
Gold Ochre DD	151.7%	61.86%	104.6%
Ultramarine Blue	35.61%	44.72%	44.66%
Kremer White	241.5%	62.91%	17.10%
Carmine	132.7%	74.83%	149.1%
Naples Yellow	50.84%	64.55%	111.1%
Viridian Green	142.0%	56.99%	52.17%
Average of 7 endmembers	113.0%	63.89%	71.18%

stands out of the other.

In Figure 4, four color patches are chosen for demonstrations. The fisrt row shows the result of colorpatch #36 and colorpatch #2. The second shows the result of colorpatch #159 and colorpatch #94. We choose to demonstrate these

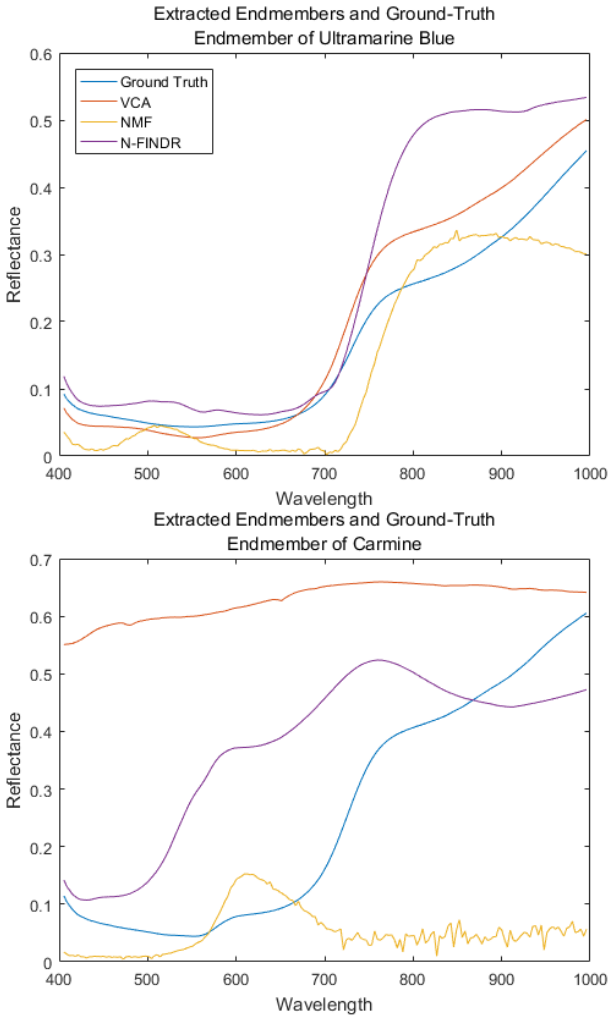

Figure 3: Ground-truth endmembers and endmembers extracted by applying VCA, NMF, N-FINDR

Table 5: Statistics of the Percentage of SAVD of each method

Statistics of the percentage of SAVD (%)				
Method	Min	Max	Mean	Std
VCA	48.7	200.0	151.1	41.3
NMF	41.6	200.0	157.2	48.6
N-FINDR	50.0	200.0	146.1	44.8

four colorpatches in such standard: VCA has the smallest SAVD in colorpatch #36, the largest SAVD in colorpatch #2. N-FINDR has the smallest SAVD in colorpatch #159, the largest SAVD in colorpatch #94. For saving the space, in the following part, P1 stands *Vermilion*, P2 for *Gold Ochre DD*, P3 for *Ultramarine Blue*, P4 for *Kremer White*, P5 for *Carmine*, P6 for *Naples Yellow*, P7 for *Viridian Green*. Table 6 presents the ground truth values and the abundance values from the different method for the four

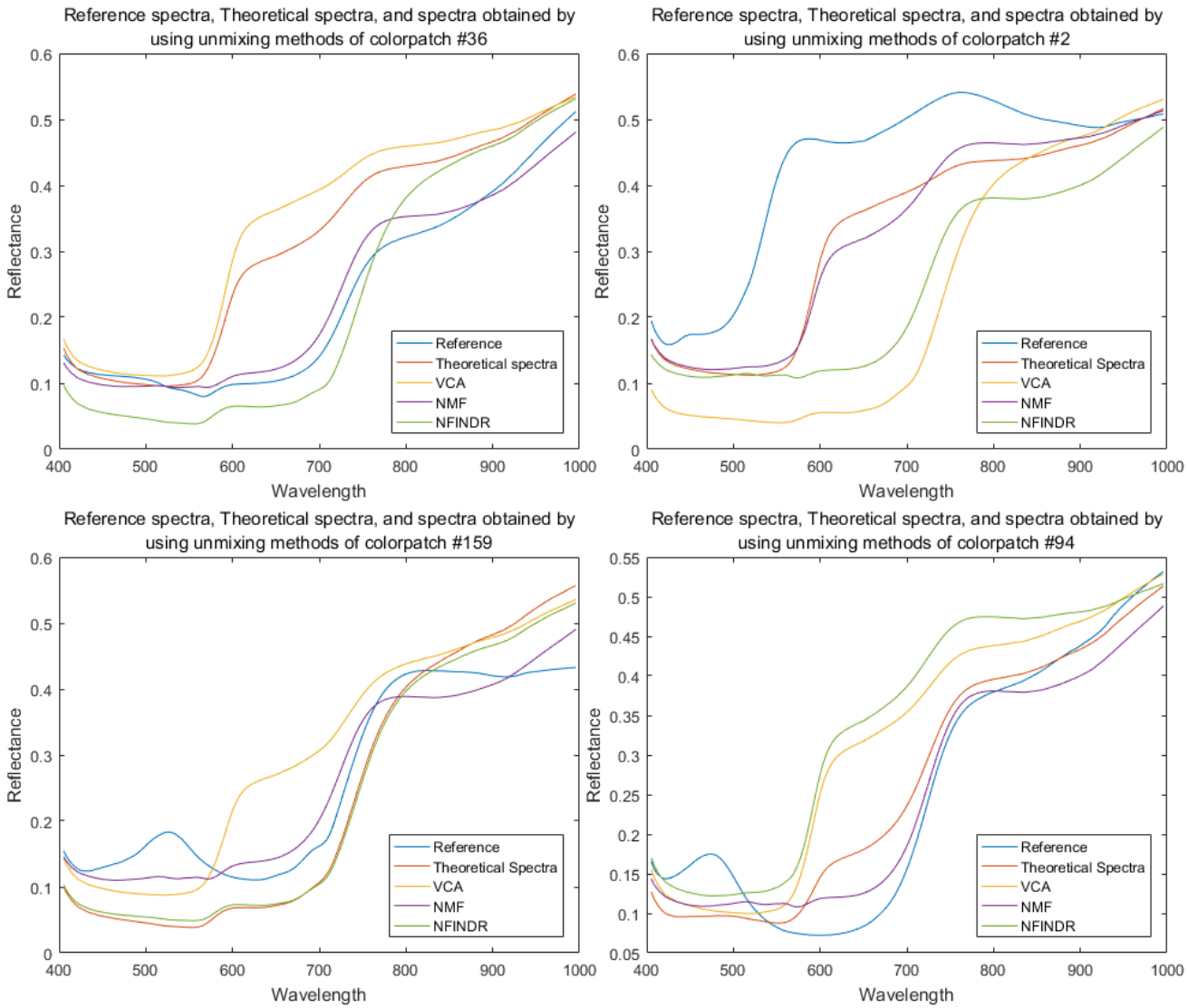

Figure 4: Reference spectra, Theoretical spectra, and spectra obtained by using unmixing methods of colorpatches

color patches presented above. The Theoretical Spectra corresponds to the linear mixing of the ground truth endmembers and abundances. The VCA, NMF and N-FINDR spectra are the linear mixing obtained with the endmembers and abundances associated to each method.

Firstly, all the Reference spectra are different form the Theoretical Spectra. This differences originate from the fact that the mixing of oil painting is probably Non-linear. In fact, even though there are some researches concerning this, researchers still cannot find the most accurate Abundance Estimation Model for oil painting. This phenomenon can explain why in Table 5, all the results of Abundance Estimation are poor. Indeed, the Linear Mixing Model suppose no macroscopic interaction between the endmembers. Yet, the pigment are mixed before being applied on the canvas.

Secondly, the color patch #2 corresponds to an endmember of the N-FINDR method while the color patch #94 corresponds to an endmember of the NMF method. If the NMF endmember is close to both the Reference and the Theoretical Spectra, it is not the case of the N-FINDR from color patch #2. This suggest that the endmember extracted are not reliable to estimate abundance.

Indeed, even though, some estimated combination are very close the the Reference (NMF in color patch #36) or the Theoretical Spectra (N-FINDR in color patch #159), the estimated abundance are far from the ground truth, neither the number not the selected pigments are a match. In Cultural Heritage, the goal is to know the pigments used by the painter. There was no constraint on the number of pigment present in the mixing during the endmember extraction. Nonetheless, we know the maximum pigment in a mix is three. Adding this constrain could improved the results.

Table 6: The percentage of Abundances of different colorpatches

Percentage of Abundances of colorpatches (%)							
Colorpatch	P1	P2	P3	P4	P5	P6	P7
#36							
Theory	50	25	0	0	25	0	0
VCA	68	24	6	0	2	0	0
NMF	4	0	28	68	0	0	0
N-FINDR	0	36	6	0	0	0	58
#2							
Theory	67	33	0	0	0	0	0
VCA	0	0	31	0	0	16	53
NMF	52	0	0	48	0	0	0
N-FINDR	0	0	100	0	0	0	0
#159							
Theory	0	25	0	0	25	0	50
VCA	46	14	11	0	17	0	12
NMF	5	0	0	95	0	0	0
N-FINDR	0	27	2	16	0	0	55
#94							
Theory	25	0	25	0	0	50	0
VCA	57	16	11	0	16	0	0
NMF	0	0	0	100	0	0	0
N-FINDR	59	0	0	41	0	0	0

5 Conclusion

In this article, we have presented and implemented several methods in Endmember Extraction originating from the field of remote sensing. It is scarce and novel that they are adapted and applied upon paintings data set. This paper has demonstrated the possibilities and usefulness in applying the unmixing methods upon the domain of cultural heritage.

To continue this work, a first direction is to look into constraint the number of pigment in the Abundance Extraction. Another possibility is to explore the Non Linear Mixing Models as the paintings extraction shows more interaction between endmembers. Or we could focus on where these interaction comes from. Creating a painting data set with more similar to remote sensing case (pointillism) could give better results with Linear Mixing Models.

6 Acknowledgement

CHANGE is funded by the European Union's Horizon 2020 programme under the Marie Skłodowska-Curie grant agreement No 813789

References

[1] Adams, J., Smith, M. & Johnson, P. Spectral mixture modeling: A new analysis of rock and soil types at the Viking Lander 1 site. *Journal Of Geophysical Research: Solid Earth*. Vol. 91, pp. 8098-8112, 1986.

[2] Albright, R., Cox, J., Duling, D., Langville, A. N., Meyer, C., Algorithms, initializations, and convergence for the nonnegative matrix factorization, *Tech. rep. 919. NCSU Technical Report Math 81706*, http://meyer. math. ncsu. edu/Meyer/Abstracts/Publications. html, 2006.

[3] Bektaş, S., Şişman, Y., The comparison of L11 and L22-norm minimization methods, *International journal of physical sciences*, Vol. 5, pp. 1721-1727, 2010.

[4] Bioucas-Dias, J. M., Plaza, A., Dobigeon, N., Parente, M., Du, Q., Gader, P., & Chanussot, J., Hyperspectral unmixing overview: Geometrical, statistical, and sparse regression-based approaches, *IEEE journal of selected topics in applied earth observations and remote sensing*, Vol. 5, pp. 354-379, 2012.

[5] Chang, C. I., *Hyperspectral Data Processing: Algorithm Design and Analysis* (1st ed., Vols. 201–206). John Wiley Sons, 2013.

[6] Chang, C. I., Chen, S. Y., Li, H. C., Chen, H. M., Wen, C. H., Comparative study and analysis among ATGP, VCA, and SGA for finding endmembers in hyperspectral imagery, *IEEE Journal of Selected Topics in Applied Earth Observations and Remote Sensing*, Vol. 9, pp. 4280-4306, 2016.

[7] Cui, C., Li, Y., Liu, B., Li, G., A new endmember preprocessing method for the hyperspectral unmixing of imagery containing marine oil spills, *ISPRS International Journal of Geo-Information*, Vol. 6, pp. 286, 2017.

[8] Dalla Mura, M., Chanussot, J., Plaza, A., An overview on hyperspectral unmixing, 2014.

[9] De Myttenaere, A., Golden, B., Le Grand, B., Rossi, F., Mean absolute percentage error for regression models, 2014. *Neurocomputing*, Vol. 192, pp. 38-48, 2016.

[10] Deborah, H., Ulfarsson, M. & Sigurdsson, J. Fully constrained least squares linear spectral unmixing of the Scream (VERSO, 1893). *IEEE Workshop on Hyperspectral Imaging and Signal Processing: Evolution in Remote Sensing (WHISPERS)*, Virtual Conference, March 2021

[11] Dennison, P. & Roberts, D. The effects of vegetation phenology on endmember selection and species mapping in southern California chaparral. *Remote Sensing Of Environment*. Vol. 87, pp. 295-309, 2003.

[12] Grillini, F., Thomas, J. & George, S. Linear, Subtractive and Logarithmic Optical Mixing Models in Oil Painting.. *CVCS*. 2020.

[13] Grillini, F., Thomas, J. B., George, S., Comparison of Imaging Models for Spectral Unmixing in Oil Painting, *Sensors*, Vol. 21, pp. 2471, 2021.

[14] Halimi, A., Altmann, Y., Dobigeon, N., Tourneret, J. Y., Nonlinear unmixing of hyperspectral images using a generalized bilinear model, *IEEE Transactions on Geoscience and Remote Sensing*, Vol. 49, pp. 4153-4162, 2011.

[15] Kim, S., Kim, H., A new metric of absolute percentage error for intermittent demand forecasts, *International Journal of Forecasting*, Vol. 32, pp. 669-679, 2016

[16] Kruse, F. A., Richardson, L. L., Ambrosia, V. G., The annals of mathematical statistics, *In Presented at the Fourth International Conference on Remote Sensing for Marine and Coastal Environments*, Vol. 17, pp. 19, 1997.

[17] Kullback, S., Leibler, R. A., Techniques developed for geologic analysis of hyperspectral data applied to near-shore hyperspectral ocean data, *IEEE signal processing magazine*, Vol. 22, pp. 79-86, 1951.

[18] Lee, D. D., Seung, H. S., Learning the parts of objects by non-negative matrix factorization, *Nature*, Vol. 401, pp. 788-791, 1999.

[19] Licciardi, G. A., Del Frate, F., Pixel unmixing in hyperspectral data by means of neural networks, *IEEE transactions on Geoscience and remote sensing*, Vol. 49, pp. 4163-4172, 2011.

[20] Lu, X., Wu, H., Yuan, Y., Yan, P., Li, X., Manifold regularized sparse NMF for hyperspectral unmixing, *IEEE Transactions on Geoscience and Remote Sensing*, Vol. 51, pp. 2815-2826, 2012.

[21] Nascimento, J. M., Dias, J. M. , Vertex component analysis: A fast algorithm to unmix hyperspectral data, *IEEE transactions on Geoscience and Remote Sensing*, Vol. 43, pp. 898-910, 2005.

[22] Pérez-Cruz, F., Kullback-Leibler divergence estimation of continuous distributions, *2008 IEEE international symposium on information theory*, pp. 1666-1670, 2008.

[23] Stein, P., A note on the volume of a simplex, *The American Mathematical Monthly*, Vol. 73, pp. 299-301, 1966.

[24] Wang, Z., Zhuang, L., Gao, L., Marinoni, A., Zhang, B., Ng, M. K., Hyperspectral Nonlinear Unmixing by Using Plug-and-Play Prior for Abundance Maps, *Remote Sensing*, Vol. 12, pp. 4117, 2020.

[25] Winter, M. E., N-FINDR: An algorithm for fast autonomous spectral end-member determination in hyperspectral data, *Imaging Spectrometry V*, Vol. 3753, pp. 266-275, 1999.

[26] Xu, Z., Zhao, H., A new spectral unmixing algorithm based on spectral information divergence, *In Seventh International Symposium on Instrumentation and Control Technology: Sensors and Instruments, Computer Simulation, and Artificial Intelligence*, Vol. 7127, pp. 712-726, 2008.

[27] Yang, C., Everitt, J. & Bradford, J. Airborne hyperspectral imagery and linear spectral unmixing for mapping variation in crop yield. *Precision Agriculture*. **8**, pp. 279-296, 2007

[28] Yuhas, R. H., Goetz, A. F., Boardman, J. W. , Discrimination among semi-arid landscape endmembers using the spectral angle mapper (SAM) algorithm, *Proc. Summaries 3rd Annu. JPL Airborne Geosci. Workshop*, Vol. 1, pp. 147-149, 1992.